DIS Results from HERA

C.M. Ginsburg
The Ohio State University, Physics Department, Columbus, OH 43210-1106, USA
on behalf of the ZEUS and H1 Collaborations

ZEUS and H1 experimental results from deep inelastic scattering at the HERA electron-proton collider are reviewed. The status of proton structure function measurements is summarized. Next-to-leading-order perturbative QCD tests are described, including several studies of the gluon density in the proton and the strong coupling constant. Recent neutral and charged current cross-section measurements at highest momentum transfers showing sensitivity to valence quark densities and electroweak effects are also presented.

1 Introduction

Deep inelastic scattering (DIS) provides a wealth of information about nucleon structure. Very high momentum transfers in DIS have been achieved at the HERA collider at DESY, where 820(920) GeV protons have been collided with 27.5 GeV positrons or electrons for a center-of-mass energy $\sqrt{s}$=300(318) GeV. The kinematic variables used to describe the $e^{\pm}p$ DIS process are x, the struck parton momentum fraction; y, the fractional energy transfer in the proton rest frame (inelasticity); and Q^2, the negative four-momentum transfer squared, where $Q^2 = sxy$. Neutral current (NC) DIS events are characterized by the exchange of a photon or Z-boson, and have a positron and a jet (or jets) in the final state. The outgoing positron and the hadronic matter are balanced in transverse momentum. Charged current (CC) DIS events are characterized by the exchange of a W-boson, and contain an undetected neutrino appearing as missing transverse momentum, and a jet (or jets) in the final state.

ZEUS [1] and H1 [2] are multi-purpose magnetic detectors. Through the end of 1999, ZEUS and H1 had collected $\sim 70-80$ pb^{-1} of luminosity, $\sim 20\%$ of which was in e^-p mode, the remainder in e^+p mode. ZEUS and H1 DIS results are described in the following, roughly in order of increasing Q^2.

2 Structure Function Formalism

To lowest order (QED Born level) the NC DIS ($e^{\pm}p \to e^{\pm}X$) cross section is

$$\frac{d^2\sigma^{\rm NC}(e^{\pm})}{dx\,dQ^2} = \frac{2\pi\alpha^2}{xQ^4}\left[Y_+\,F_2^{\rm NC} \mp Y_-\,xF_3^{\rm NC} - y^2\,F_L^{\rm NC}\right] \equiv \frac{2\pi\alpha^2}{xQ^4}\tilde{\sigma}^{\rm NC}(e^{\pm}) \qquad (1)$$

where $Y_{\pm} = 1 \pm (1-y)^2$, and $\tilde{\sigma}^{\rm NC}(e^{\pm})$ is the reduced NC cross section. In lowest-order QCD, the structure functions $F_2^{\rm NC}$ and $xF_3^{\rm NC}$ are the sums over quark flavor of the product of quark couplings and momentum densities. The quark couplings depend on quark charges and the electroweak (EW) parameters M_Z, $\sin^2\theta_W$, etc. For low Q^2, i.e., $Q^2 \ll M_Z^2$, only γ exchange is significant, the $xF_3^{\rm NC}$ contribution is small, and the cross section is sensitive to $F_L^{\rm NC}$ for $y \gtrsim 0.5$. At higher Q^2, i.e., $Q^2 \gtrsim M_Z^2$, both γ and Z exchange are important, the F_L contribution is small, and the cross section is sensitive to $xF_3^{\rm NC}$.

The QED Born-level CC DIS ($e^\pm p \to \overset{(-)}{\nu} X$) cross sections are

$$\frac{d^2\sigma^{\rm CC}(e^+)}{dx\, dQ^2} = \frac{G_F^2 P_W^2}{4\pi}\left[(\bar{u}+\bar{c}) + (1-y)^2(d+s)\right] \equiv \frac{G_F^2 P_W^2}{4\pi x}\tilde{\sigma}^{\rm CC}(e^+), \quad (2)$$

$$\frac{d^2\sigma^{\rm CC}(e^-)}{dx\, dQ^2} = \frac{G_F^2 P_W^2}{4\pi}\left[(u+c) + (1-y)^2(\bar{d}+\bar{s})\right] \equiv \frac{G_F^2 P_W^2}{4\pi x}\tilde{\sigma}^{\rm CC}(e^-), \quad (3)$$

where $P_W \equiv M_W^2/(Q^2+M_W^2)$, and $\tilde{\sigma}^{\rm CC}(e^\pm)$ is the reduced CC cross section. Note that the e^- and e^+ couple to different quark flavors; at high Q^2 and high x, the e^+p CC cross section is most sensitive to the d quark, whereas the e^-p CC cross section is most sensitive to the u quark.

3 DIS Results from HERA

Both the NC and CC cross sections agree well with Standard Model (SM) expectations. The $F_2^{\rm NC}$ structure function [3] and a next-to-leading-order (NLO) fit [4] are shown in Fig. 1(left), as a function of Q^2 in bins of x over five orders of magnitude in Q^2 and four orders of magnitude in x. Scaling is observed in the region $x \sim 0.1$ for Q^2 at least up to ~ 5000 GeV^2. Scaling violations, which occur in NLO QCD due to the presence of the gluon, are shown to be positive with increasing Q^2 for $x \lesssim 0.1$ and negative for $x \gtrsim 0.1$. The e^+p CC DIS reduced cross section [5] is shown in Fig. 1(right). The SM expectation [6,7] is in good agreement with the data; at high x, the valence d and s quarks (dashed curves) dominate $\tilde{\sigma}^{\rm CC}$, whereas at lower x the $\bar{u}$ and $\bar{c}$ sea quarks (dotted curves) dominate.

The $F_2^{\rm NC}$ measurement has been extended to lower Q^2 and lower x by ZEUS with the addition of detectors at small $e^\pm$ scattering angles. The resulting $F_2^{\rm NC}$ is shown [8] with other low-Q^2 data [3,4,9] as a function of x in Q^2 bins in Fig. 2(left). $F_2^{\rm NC}$ as a function of Q^2 in y bins is shown in Fig. 2(right). At the Q^2 values of this measurement, $Q^2 \lesssim 1$ GeV^2, $F_2^{\rm NC}$ rises slowly with decreasing x, and is well described by the Regge parametrization. In addition, $F_2^{\rm NC}$ at low Q^2 exhibits a strong Q^2 dependence, approaching $F_2^{\rm NC} \propto Q^2$ at the lowest Q^2 values.

In addition to $F_2^{\rm NC}$ scaling violations, the boson-gluon fusion (BGF) process is inherently sensitive to the gluon in the proton, see Fig. 3(left). BGF

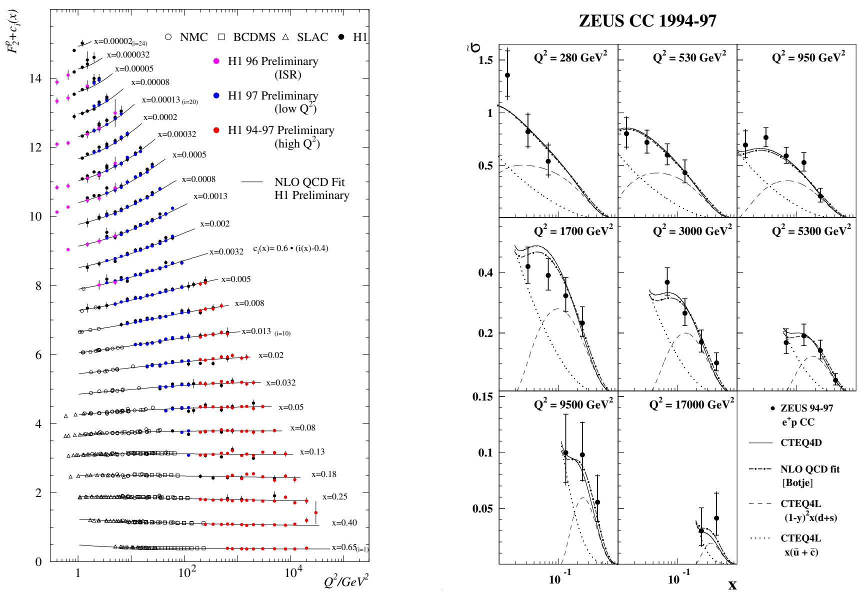

Figure 1: $F_2^{\rm NC}$ as a function of Q^2 in x bins (left); and the reduced CC cross section, $\tilde{\sigma}^{\rm CC}$, as a function of x in Q^2 bins (right).

dominates in inclusive D^* production and in dijet production, so these processes may be used to study the gluon.

$F_2^{c\bar{c}}$ has been extracted from the inclusive NC DIS D^* production cross section [10]. In Fig. 3(center), $F_2^{c\bar{c}}$ is shown as a function of Q^2 in x bins. In Fig. 3(right), the fractional charm content in the proton, $F_2^{c\bar{c}}/F_2^{\rm NC}$, is shown as a function of x in Q^2 bins. Also shown in the figures is an NLO QCD fit, where the error band is dominated by assumed variations of the c-quark mass. The NLO QCD fits agree well with these data, indicating a consistent gluon picture in scaling violations and BGF. Strong scaling violations are seen in $F_2^{c\bar{c}}$, indicating a rising gluon down to the lowest x measured. In addition, the rise of $F_2^{c\bar{c}}$ is stronger than that of $F_2^{\rm NC}$, and an increase of the proton charm content with Q^2 is observed. The gluon density may be extracted from a fit to D^* cross sections in DIS [3], as shown in Fig. 4(left). A steep rise of the gluon for decreasing x is seen; furthermore, the results agree well with the gluon extracted from NLO QCD fits to $F_2^{\rm NC}$ scaling violations.

Dijet production also provides valuable information on the gluon. From an NLO QCD fit to the distributions $d^2\sigma_{\rm dijet}/dQ^2d\xi$ and $d^2\sigma_{\rm dijet}/dQ^2dx$, where $\xi \equiv x(1 + M_{jj}^2/Q^2)$ and M_{jj} is the invariant mass of the two jets, the gluon

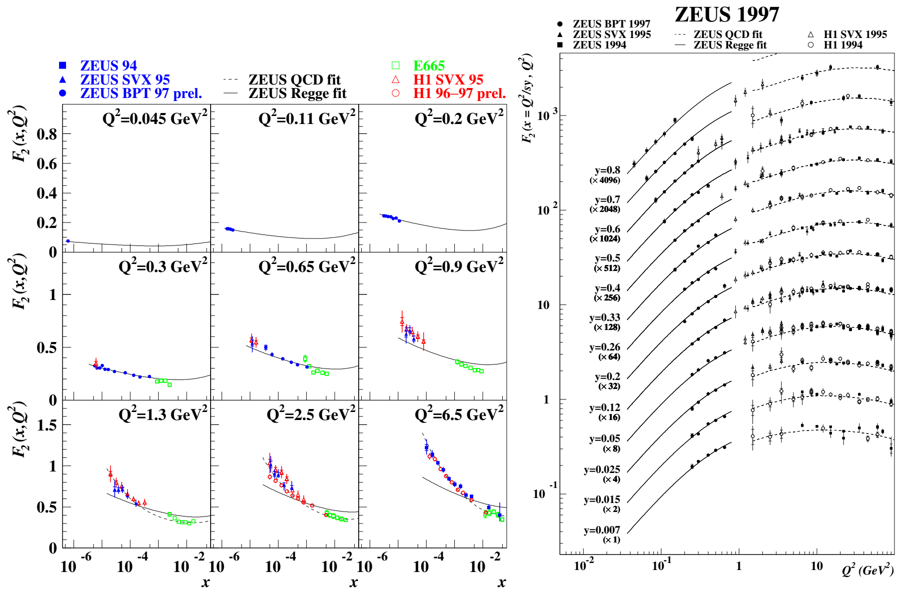

Figure 2: $F_2^{\rm NC}$ as a function of x in Q^2 bins (left); and $F_2^{\rm NC}$ as a function of Q^2 in y bins (right). Also shown are a Regge-type (Reggeon + Pomeron) fit, and an NLO QCD fit.

density is extracted [11], as shown in Fig. 4(right). The quark densities are constrained from $F_2^{\rm NC}$ measurements, and α_s is allowed to vary within the errors of its world-average value [12]. The resulting gluon is consistent with that from NLO QCD fits to $F_2^{\rm NC}$ and $F_2^{c\bar{c}}$, but only H1 data are required (no fixed-target data for example).

The strong coupling constant has been measured [13] using an NLO QCD fit to the inclusive jet cross section, $d^2\sigma_{\rm jet}/dE_T dQ^2$, with the result $\alpha_s(M_Z) = 0.1181 \pm 0.0030(\mathrm{exp})^{+0.0039}_{-0.0046}(\mathrm{th})^{+0.0036}_{-0.0015}(\mathrm{pdf})$, where the errors are experimental, theoretical, and due to parton momentum densities, respectively. This may be compared to the world-average value [12] of $\alpha_s(M_Z) = 0.119 \pm 0.004$. By measuring the single differential cross sections from this analysis, the running of α_s as a function of E_T and Q, is shown to be consistent with the SM expectation, as demonstrated in Fig. 5.

At large Q^2, the NC and CC cross sections are sensitive to the Z and W masses, respectively. The sensitivity of the NC cross section to the Z mass is demonstrated [14] in Fig. 6(left), where the differential cross section as a function of x is shown for both e^+p and e^-p running mode. In both cases, the world-average value [15] ($M_Z = (91.187 \pm 0.007)$ GeV) is clearly favored over a model

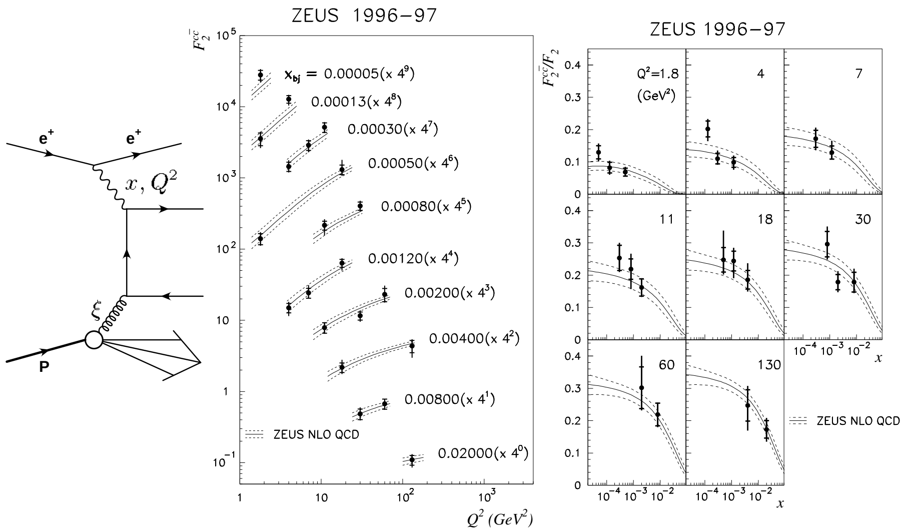

Figure 3: Boson-gluon fusion diagram (left), $F_2^{c\bar{c}}$ as a function of Q^2 in x bins (center) and the fraction of charm content in the proton, $F_2^{c\bar{c}}/F_2^{\rm NC}$, as a function of x in Q^2 bins (right). Also shown is an NLO QCD fit, where the error band is dominated by variations in m_c.

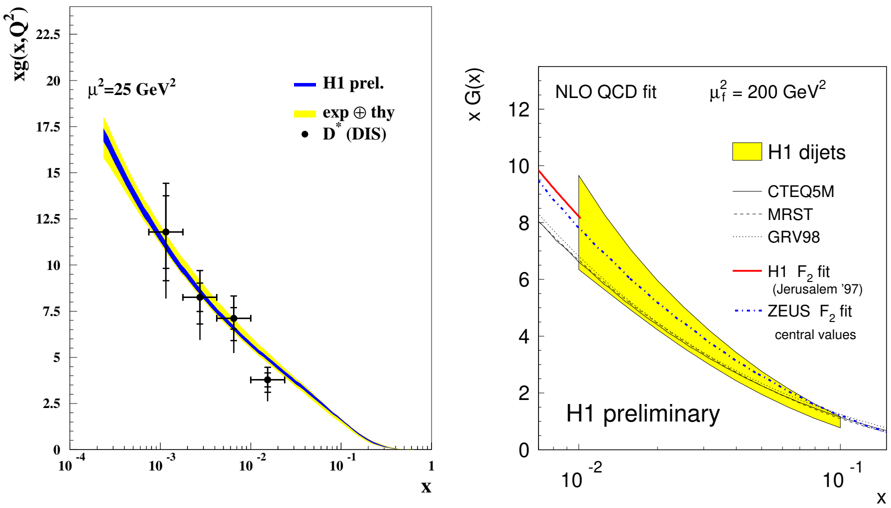

Figure 4: Gluon density from $D^\star$ production (left) and from dijet production (right).

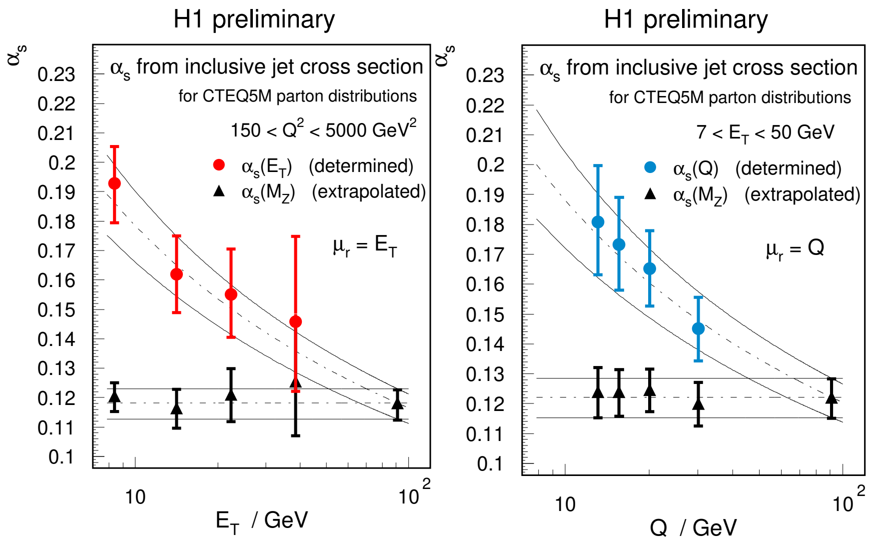

Figure 5: Running of α_s as a function of E_T (left) and Q (right) compared to the expectation (dashed curves). The rightmost point in both plots is the result of the combined fit.

which ignores the Z contribution ($M_Z = \infty$). In CC DIS, the sensitivity of the cross section to the EW propagator mass is higher than in the NC case. The M_W may be extracted by a χ^2 fit to the measured cross sections with fixed [15] $G_F = 1.16639 \times 10^{-5}$ GeV^{-2} with the result [5,16]

$$M_W = 81.4^{+2.7}_{-2.6}(\text{stat.}) \pm 2.0(\text{syst.})^{+3.3}_{-3.0}(\text{pdf}) \text{ GeV (ZEUS), and} \quad (4)$$

$$M_W = 80.9 \pm 3.3(\text{stat.}) \pm 1.7(\text{syst.}) \pm 3.7(\text{pdf}) \text{ GeV (H1),} \quad (5)$$

as shown in Fig. 6(right). These may be compared with the world-average value [15] of $M_W = (80.41 \pm 0.10)$ GeV. The agreement between these Z and W masses and the masses extracted through timelike production in e^+e^- and $\bar{p}p$ data confirms the SM prediction in the spacelike regime.

At very high Q^2, the EW interaction may be observed through its effect on the NC cross section; the $\gamma - Z$ interference term is destructive in e^+p mode and constructive in e^-p mode. The ratio of e^-p to e^+p NC differential cross sections [14] is shown as a function of Q^2 in Fig. 7(left), where the $\gamma - Z$ interference is observed. The $e^{\pm}p$ NC reduced cross sections are shown as a function of Q^2 in x bins in Fig. 7(right), where the interference effect is also demonstrated. In both plots, the NLO QCD fits [4,6,7] made at low Q^2 and evolved to higher Q^2 agree well with the data.

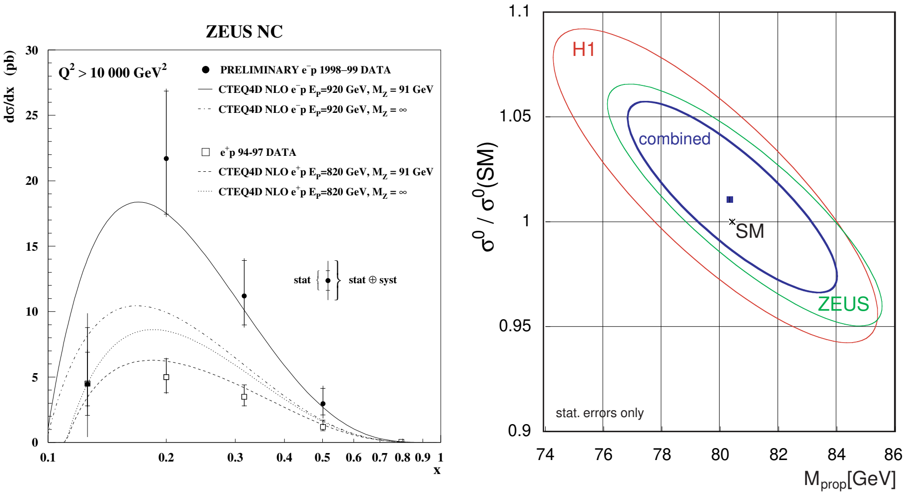

Figure 6: Sensitivity of the NC differential cross section $d\sigma/dx$ to M_Z (left); and CC cross section divided by SM prediction vs. M_W measured from the CC cross section (right).

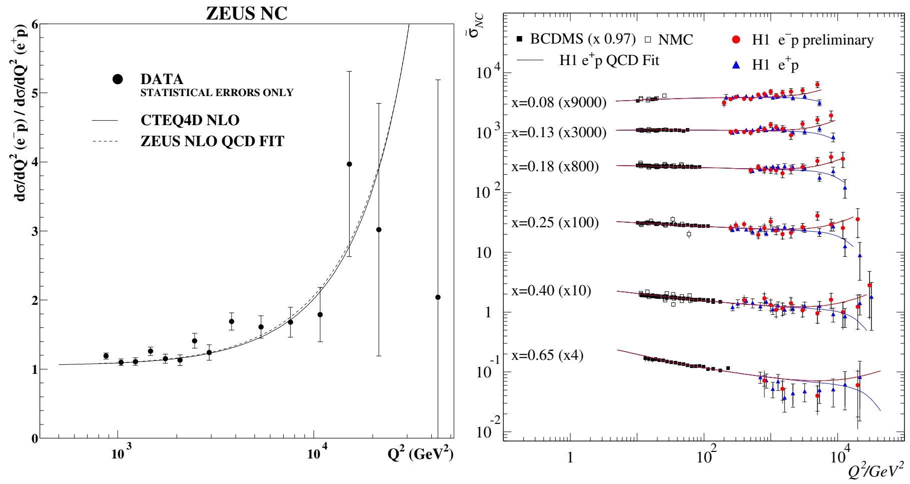

Figure 7: NC differential cross section as a function of Q^2 (left); and NC reduced cross section as a function of Q^2 in x bins (right).

4 Conclusions

The ZEUS and H1 experiments are testing QCD and measuring proton structure over ~6 orders of magnitude in Q^2 and x. At low Q^2, DIS probes the transition between soft physics and QCD. For $Q^2 \gtrsim 1$ GeV^2, NLO QCD describes the data very well; several different data sets provide a consistent gluon density, and the extracted α_s agrees well with complementary measurements. Also, EW effects observed at highest Q^2 are consistent with the SM prediction.

HERA begins its luminosity upgrade in September 2000, after which ZEUS and H1 are each expected to record ~1000 pb^{-1} of luminosity. This large data set will provide the possibility for higher precision measurements at medium and high Q^2, of the valence quark densities in the proton, and of EW effects. In addition, it will open up greater discovery potential for exotic signatures.

References

1. ZEUS Collaboration, The ZEUS Detector Status Report, DESY 1993.
2. H1 Collaboration, I. Abt *et al.*, DESY preprint 93-103 (July 1993) 194 pp.; *idem Nucl. Instrum. Methods* A 386, 310 (1997); H1 SPACAL Group, R.D. Appuhn *et al.*, *Nucl. Instrum. Methods* A 386, 397 (1997).
3. H1 Collaboration, Contribution to Lepton-Photon 1999, Stanford; *ibid.* M. Klein plenary talk.
4. H1 Collaboration, S. Aid *et al.*, Nucl. Phys. B470 (1996) 3.
5. ZEUS Collaboration, J. Breitweg *et al.*, Eur. Phys. J. C12 (2000) 411.
6. ZEUS Collaboration, J. Breitweg *et al.*, Eur.Phys. J. C7 (1999) 609; M. Botje, DESY-99-038 (Dec 1999), *hep-ex/9910045.*
7. H.L. Lai *et al.*, Phys. Rev. D 55 (1997) 1280.
8. ZEUS Collaboration, J. Breitweg *et al.*, DESY 00-071 (May 2000), submitted to Physics Letters B.
9. ZEUS Collaboration, M. Derrick *et al.*, Z. Phys. C 72 (1996) 399; E665 Collaboration, M.R. Adams *et al.*, Phys. Rev. D 54 (1996) 3006; ZEUS Collaboration, J. Breitweg *et al.*, Phys. Lett. B 407 (1997) 432; H1 Collaboration, C. Adloff *et al.*, Nucl. Phys. B497 (1997) 3; ZEUS Collaboration, J. Breitweg *et al.*, Eur. Phys. J. C7 (1999) 609.
10. ZEUS Collaboration, J. Breitweg *et al.*, Eur. Phys. J. C12 (2000) 35.
11. H1 Collaboration, Contribution to ICHEP 98, Vancouver, Abs. 520.
12. S. Bethke, *hep-ex/9812026.*
13. H1 Collaboration, Contribution to EPS 99, Tampere, Abs. 157.
14. ZEUS Collaboration, Contribution to EPS 99, Tampere, Abs. 549.
15. C. Caso et al., Eur. Phys. J. C3 (1998) 1.
16. H1 Collaboration, C. Adloff *et al.*, Eur. Phys. J. C13 (2000) 609.